

# Vertex corrections to the optical conductivity in the square lattice Hubbard model and their role for the high-temperature transport

J. Vučičević,<sup>1</sup> J. Kokalj,<sup>2,3</sup> R. Žitko,<sup>3,4</sup> N. Wentzell,<sup>5</sup> D. Tanasković,<sup>1</sup> and J. Mravlje<sup>3</sup>

<sup>1</sup>*Scientific Computing Laboratory, Center for the Study of Complex Systems, Institute of Physics Belgrade, University of Belgrade, Pregrevica 118, 11080 Belgrade, Serbia*

<sup>2</sup>*University of Ljubljana, Faculty of Civil and Geodetic Engineering, Jamova 2, Ljubljana, Slovenia*

<sup>3</sup>*Jozef Stefan Institute, Jamova 39, SI-1000, Ljubljana, Slovenia*

<sup>4</sup>*University of Ljubljana, Faculty of Mathematics and Physics, Jadranska 19, Ljubljana, Slovenia*

<sup>5</sup>*Center for Computational Quantum Physics, Simons Foundation Flatiron Institute, New York, NY 10010 USA*

Calculating transport properties presents a great challenge in the study of strongly correlated electrons, particularly in two dimensions where the non-local processes and the vertex corrections are important, but remain poorly understood. We study the Hubbard model on the square lattice in the strongly correlated regime. We use several complementary state-of-the-art numerical methods to disentangle the different effects and resolve the problem conclusively at high temperatures. In this regime, non-local correlations and long-distance quantum fluctuations have little impact, yet the vertex corrections survive and substantially suppress resistivity. Our study becomes particularly relevant in the light of recent experiments on optical lattices that provide realizations of the two-dimensional Hubbard model in a similar parameter regime.

A famous saying is that the electronic transport is the first property to be measured, last to be understood<sup>1</sup>. Yet, recently there has been progress both from the field-theoretical point of view<sup>2,3</sup> as well as from the numerical simulations of the lattice models<sup>4–11</sup>. The dynamical mean-field theory (DMFT)/high-temperature expansion approach<sup>9</sup> and exact diagonalization using finite temperature Lanczos method (FTLM)<sup>10</sup> both found a growth of resistivity beyond the Mott-Ioffe-Regel value<sup>12</sup> (which in the Boltzmann picture corresponds to a scattering at every atom). This does not come from a further suppression of the electronic lifetime<sup>5,6</sup>, but rather indicates a suppression of the charge susceptibility<sup>9,10</sup>. The same phenomenology was found also in lattice simulations using Monte Carlo techniques<sup>11</sup>. Importantly, recent experiments on the optical lattice realizations of the Hubbard model confirmed these results<sup>13</sup>.

It is useful to recall that the mentioned numerical approaches fall into two distinct classes: *A*) one solves an isolated finite cluster of lattice sites, as representative of the thermodynamic limit;<sup>10,11,14</sup> *B*) one solves an effective, self-consistently determined “embedded” cluster, which provides propagators of infinite range, yet limits the range of electronic correlations.<sup>15–23</sup> The diagrammatic content of the self-energy in the two approaches is sketched in Fig. 1a. Approach *B* captures longer distance quantum fluctuations, and is therefore assumed to converge more quickly with cluster size at the price of an iterative solution of the (embedded) cluster, as opposed to the “single-shot” calculation in the approach *A*.

The DMFT approximates the self-energy by a purely local quantity (the embedded cluster contains a single

site), neglecting all but local correlations. Hence, the fact that DMFT and the  $4 \times 4$  lattice FTLM give qualitatively similar results for resistivity, both close to the optical lattice experiment<sup>13</sup>, suggests that the correlations are local, and quantum fluctuations (i.e. the excursions of electrons in the lattice) short ranged. This result is not trivial: while the thermodynamic charge susceptibility is expected to recover the atomic limit at high temperature, the same does not necessarily hold for the self-energies nor the general two-particle quantities<sup>9</sup>.

At a quantitative level, however, the DMFT and FTLM  $4 \times 4$  lattice resistivities do differ beyond the numerical/statistical error bars of the methods.<sup>13</sup> Does this

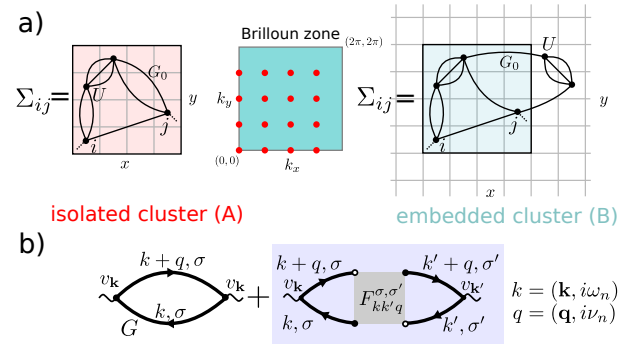


FIG. 1. (a) Illustration of the type of self-energy diagrams that are captured by isolated cluster and embedded cluster (in particular cellular DMFT), and the respective difference in the Brillouin zone (discrete vs. continuous). (b) Separation of a susceptibility into the bubble and the vertex corrections part.

mean that *non-local correlations* persist in this regime? These are encoded in the non-local corrections to self-energy, present in FTLM, but beyond the DMFT approximation. Or is it that *quantum fluctuations* at distances beyond the linear size of the FTLM cluster play a role? DMFT does capture these through an effective fermionic bath. Finally, it could as well be *the vertex corrections*. Namely, as shown in Fig. 1b, the two-particle correlation functions can be split into the disconnected part (“the bubble”) and the connected part (“vertex corrections”). In Ref.<sup>13</sup>, the DMFT result contains only the bubble contribution, while the FTLM is the full result. Whereas the contribution of the connected part is always important for charge susceptibility<sup>24–26</sup>, in the large dimensionality limit the vertex corrections to conductivity cancel<sup>27</sup> (the full vertex  $F$  loses  $\mathbf{k}\mathbf{k}'$ -dependence and the current vertex is odd  $v_{-\mathbf{k}} = -v_{\mathbf{k}}$ , unlike the charge vertex which is even). In finite dimensions, however, the vertex corrections do contribute to conductivity, as discussed previously in several approximative approaches<sup>28–33</sup>. In numerically exact solutions of the Hubbard model, no firm understanding of the effect of vertex corrections to conductivity has emerged so far.

To answer these questions, we study the conductivity and the charge susceptibility in the Hubbard model on a square lattice using several computational methods from both approaches at different cluster sizes. The comparison of the results from different methods allows us to distinguish between different contributions to the two susceptibilities of interest. We identify a characteristic temperature  $T \sim 0.3D$  above which non-local self-energy and long-distance quantum fluctuations bring a negligible contribution to the conductivity, thus rendering a straight-forward “one-shot” solution of an isolated  $4 \times 4$  cyclic cluster essentially exact. Strikingly, the bubble part captures the qualitative picture, while the vertex corrections amount for a sizable, yet roughly constant shift in dc-resistivity. Our findings not only explain the observations of recent optical lattice transport experiment, but also provide guidelines for the choice and the development of the computational methods.

*Model.* The Hamiltonian reads

$$H = -t \sum_{\sigma, \langle i, j \rangle} c_{\sigma i}^\dagger c_{\sigma j} + U \sum_i n_{\uparrow i} n_{\downarrow i} - \mu \sum_{\sigma, i} n_{\sigma i} \quad (1)$$

where  $c_{\sigma i}^\dagger/c_{\sigma i}$  create/annihilate an electron of spin  $\sigma$  at the lattice site  $i$ . The hopping amplitude between the nearest neighbors is denoted  $t$ , and we set  $D = 4t$  as the unit of energy. The density operator is  $n_{\sigma i} = c_{\sigma i}^\dagger c_{\sigma i}$ , the chemical potential  $\mu$ , and the on-site Hubbard interaction  $U$ . Throughout the paper, we keep  $U = 2.5D$ , which corresponds to the (doped) Mott insulator regime, and assume paramagnetic solutions with full lattice symmetry.

*Formalism.* The paramagnetic current-current correlation function is defined as

$$\Lambda_{\mathbf{q}}^{\alpha\beta}(i\nu_n) \equiv \sum_i e^{-i\mathbf{q} \cdot \mathbf{r}_i} \int d\tau e^{i\nu_n \tau} \langle j_i^\alpha(\tau) j_{i=0}^\beta(0) \rangle \quad (2)$$

where  $\tau$  is imaginary time,  $i\nu_n = 2in\pi T$  is bosonic Matsubara frequency,  $\mathbf{r}_i = (x_i, y_i)$  denotes the real-space vector of the site  $i$ ,  $\alpha, \beta$  denote the directions in space ( $x$  or  $y$ ), and the paramagnetic current operator  $j$  is defined as  $j_i^\alpha = -it \sum_\sigma c_{\sigma i}^\dagger c_{\sigma, \text{n.n.}(i; \alpha)} + \text{h.c.}$  where  $\text{n.n.}(i; \alpha)$  denotes the nearest neighbor in the  $\alpha$  direction. The optical conductivity is defined as<sup>34</sup>

$$\sigma_{\mathbf{q}}^{\alpha\beta}(\omega) = \frac{1}{i\omega} [\Lambda_{\mathbf{q}}^{\alpha\beta}(\omega) - \Lambda_{\mathbf{q}=0}^{\alpha\beta}(\omega=0)] \quad (3)$$

where  $\Lambda(\omega)$  is the analytical continuation of  $\Lambda(i\nu_n)$  to the real axis, i.e. the inverse of the Hilbert transform

$$\Lambda_{\mathbf{q}}^{\alpha\beta}(i\nu) = \frac{1}{\pi} \int d\omega \frac{\text{Im} \Lambda_{\mathbf{q}}^{\alpha\beta}(\omega)}{\omega - i\nu} = \frac{1}{\pi} \int d\omega \frac{\omega \text{Re} \sigma_{\mathbf{q}}^{\alpha\beta}(\omega)}{\omega - i\nu}. \quad (4)$$

We are interested in longitudinal, uniform conductivity  $\sigma_{\mathbf{q}=0}^{xx}(\omega)$ , so we adopt a shorthand notation  $\Lambda(i\nu_n) \equiv \Lambda_{\mathbf{q}=0}^{xx}(i\nu_n)$  and analogously for  $\sigma(\omega)$ . The second equality in Eq. (4) is due to  $\text{Im} \Lambda(\omega=0) = 0$  which holds in the present context. Furthermore, the direct-current (dc) conductivity is defined as  $\sigma_{\text{dc}} = \text{Re} \sigma(\omega=0) = \text{Im} \Lambda'(\omega=0)$ , and the dc resistivity is then  $\rho_{\text{dc}} = 1/\sigma_{\text{dc}}$ . The thermodynamic charge susceptibility can be evaluated from the uniform static component of the charge-correlation function

$$\begin{aligned} \chi_c &\equiv \chi_{\mathbf{q}=0}(i\nu_n=0) \\ &\equiv \sum_i \int d\tau \left\langle (n_i(\tau) - \langle n \rangle) (n_{i=0}(0) - \langle n \rangle) \right\rangle \\ &= \frac{d\langle n \rangle}{d\mu} \end{aligned} \quad (5)$$

where  $n_i = n_{\uparrow i} + n_{\downarrow i}$  is the total charge operator.

Both  $\chi_c$  and  $\Lambda$  are two-particle correlation functions and can be separated into the bubble and the vertex corrections part, Fig. 1. The respective bubbles read

$$\begin{aligned} (\chi, \Lambda^{xx})_{\mathbf{q}}^{\text{disc}}(i\nu_m) &= \\ -T \sum_{i\omega_n, \mathbf{k}, \sigma} v_{\mathbf{k}}^2 G_{\sigma, \mathbf{k}+\mathbf{q}}(i\omega_n + i\nu_m) G_{\sigma, \mathbf{k}}(i\omega_n) \end{aligned} \quad (6)$$

with the vertex factor  $v_{\mathbf{k}} = 1$  in the case of  $\chi$ , and  $v_{\mathbf{k}} = \frac{\partial \varepsilon_{\mathbf{k}}}{\partial k_x} = 2t \sin k_x$  in the case of  $\Lambda^{xx}$  on the square lattice. Here  $G$  is the full Green’s function,  $\varepsilon_{\mathbf{k}}$  denotes the bare dispersion,  $i\omega_n = i(2n+1)\pi T$  is the fermionic Matsubara frequency. In all quantities, the superscript “disc” denotes the bubble contribution, and the superscript “conn” the vertex corrections part.

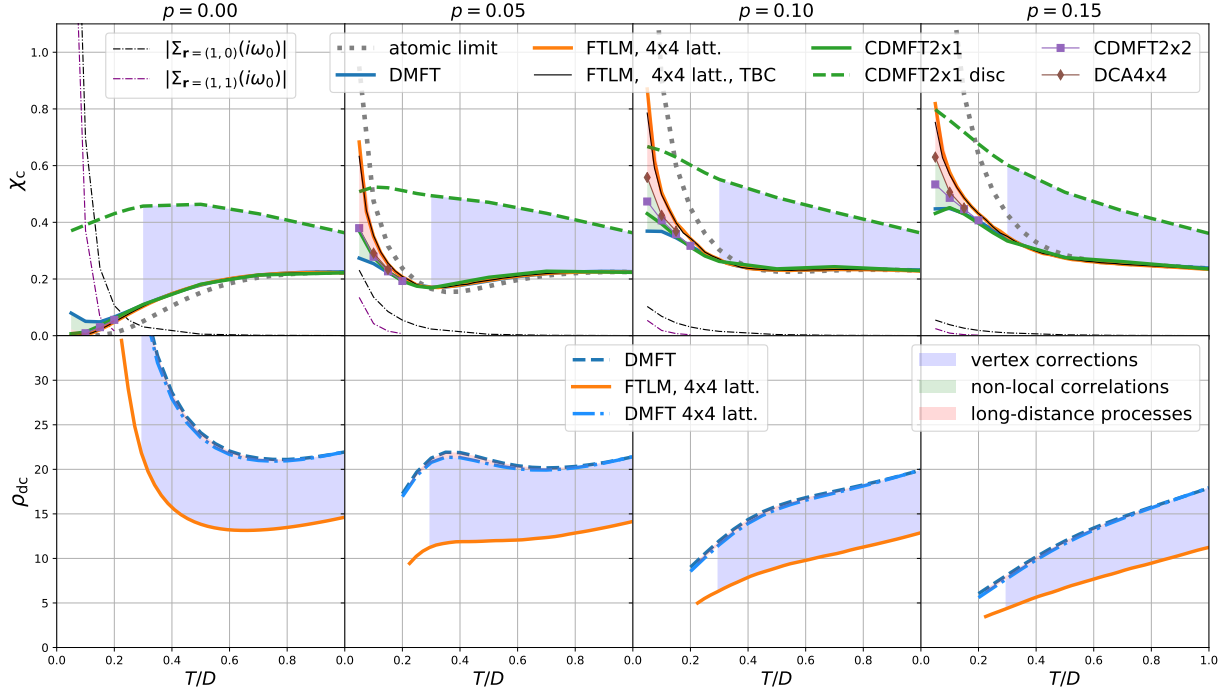


FIG. 2. Charge susceptibility (upper) and dc resistivity (lower) as a function of temperature, at different levels of doping. The color between the curves denotes the physical origin of the difference. Dashed curves denote just the bubble contribution, solid lines the full result. For orientation, the Mott-Ioffe-Regel limit is  $\rho_{\text{MIR}} \sim 3$ .

*Methods A.* We solve an isolated cyclic  $4 \times 4$  cluster using the FTLM<sup>35,36</sup> method and quantum Monte Carlo (the continuous-time interaction-expansion algorithm, CTINT<sup>18,37</sup>). Both methods yield numerically exact solutions of the representative finite-size model. In FTLM we calculate  $\sigma(\omega)$ , while CTINT yields  $\Lambda(i\nu_n)$ , as well as the self-energy  $\Sigma_{ij}(i\omega_n)$  and the Green's function  $G_{ij}(i\omega_n)$ <sup>38</sup>.

In the isolated cluster calculations one faces several finite-size effects stemming from the finite range of the bare electronic propagator<sup>35,36</sup>. Most importantly, this not only limits the range of electronic correlations, but also affects the diagrammatic content of short range correlations: diagrams with distant interaction vertices are not captured (Fig. 1). One may see this equivalently in the  $\mathbf{k}$ -space as a discretization of the Brillouin zone, which affects the internal momentum summations in all self-energy and full vertex diagrams.

*Methods B.* We solve the embedded clusters of size  $2 \times 1$  and  $2 \times 2$  within the cellular DMFT scheme (CDMFT)<sup>39</sup> and the  $4 \times 4$  cluster within the dynamical cluster approximation (DCA) scheme<sup>40</sup>, both using CTINT (unlike the isolated cluster case, the  $G_0$  entering CTINT here takes account of the effective non-interacting bath). The single-site DMFT calculations (cluster size  $N_c = 1$ ) are done using both the CTINT and the approximative real-frequency numerical renormalization group method

(NRG) as impurity solvers. The obtained thermodynamical results, self energies and optical conductivities agree closely between these two approaches (e.g. the difference in  $\rho_{\text{dc}}$  is about 2% at most).

Unlike in the isolated cluster case, in CDMFT method an electron can travel infinitely far between two scatterings, but a self-energy insertion in the corresponding diagrammatic expansion can only be of limited range (see Fig. 1). In DCA, the approximation is made in reciprocal space and amounts to allowing the electron to visit  $\mathbf{k}$ -states otherwise not present in the finite cluster.<sup>22</sup>

*Results.* Top panels of Fig. 2 show the temperature dependence of  $\chi_c$  for several values of doping  $p = 1 - \langle n \rangle$ . One sees that in the high-temperature regime  $T \gtrsim 0.3D$ , the results of different methods (solid curves) all agree. With even further increase of temperature, the value approaches that of the atomic limit, as expected of a thermodynamic quantity.

At lower temperatures, the non-local correlations show up. At half-filling  $p = 0$ , the Mott insulating, incompressible state is incorrectly described in DMFT. Away from half-filling, FTLM and DCA yield a charge susceptibility that increases with lowering temperature, yet in DMFT, it saturates instead. The enhancement of charge susceptibility at low  $T$  comes from the antiferromagnetic fluctuations<sup>10</sup>. The difference between the DCA and the DMFT is used to characterize the importance

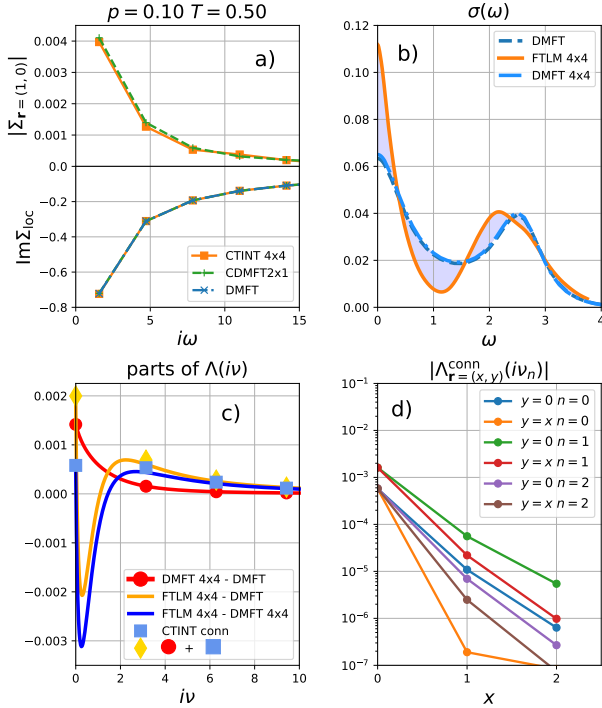


FIG. 3. All panels:  $p = 0.1$ ,  $T = 0.5D$ . a) Benchmark of self-energy in the high temperature regime. b) Comparison of the optical conductivity between various methods. c) See text. d) Real-space resolution of the vertex corrections along two directions (CTINT  $4 \times 4$  result).

of non-local correlations (green shading). They manifest themselves also in the growth of non-local self-energy at low  $T$  (thin dashed-dotted lines). The DCA and the FTLM result do not completely coincide; the difference (pink shading) comes from the longer-distance quantum fluctuations. The discretization of the Brillouin zone in FTLM can be somewhat ameliorated by the twisted-boundary conditions scheme (TBC)<sup>41</sup>. As expected, TBC is closer to DCA (black line), but one needs a better method to capture the full effect of longer-range processes.

We have also evaluated separately the bubble contribution  $\chi^{\text{conn}}$  to  $\chi_c$  (dashed lines) and observe it is substantially larger than the full result  $\chi_c$ .

Bottom panels of Fig. 2 show the temperature dependence of resistivity  $\rho_{dc}$  as calculated from the bubble term in the DMFT (dashed line) and the full result from FTLM (solid line). Strikingly, even in the temperature range  $T \gtrsim 0.3D$  where the behavior of  $\chi_c$  collapsed to that of the atomic limit, the DMFT and FTLM are shown to yield significantly different results with a lower value of resistivity found in the FTLM. To understand the origin of this difference we take a closer look of the data at  $T = 0.5$ ,  $p = 0.1$  that we show in Fig. 3. In panel a) we compare the self-energies found

in the DMFT, CDMFT  $2 \times 1$  and the CTINT calculation for the isolated  $4 \times 4$  cluster. Not only is the nearest neighbor self-energy (top) found to be two orders of magnitude smaller than the local one (bottom), but also the local parts of the self-energies show excellent agreement. Thus, neither non-local correlations (neglected in DMFT) nor long-range processes (neglected in  $4 \times 4$ ) play an important role for the self-energy at this temperature.

Might long-range processes play a more important role for the conductivity? One can readily investigate the role of long-range processes for the bubble part of the conductivity. This is done by calculating the conductivity in the DMFT formulated for the  $4 \times 4$  lattice, which amounts to discretizing the Brillouin zone (in both the self-consistency condition, and internal bubble summation Eq. 6). Fig. 3b compares the optical conductivity obtained in this way (denoted by DMFT  $4 \times 4$ ) to the infinite lattice DMFT result and to the FTLM one. The DMFT and the DMFT  $4 \times 4$  are close: the long-range processes clearly do not account for the discrepancy between the DMFT and the FTLM either. The most of the difference between the DMFT and the FTLM result thus comes from the vertex corrections. It is striking to see that the locality of self-energy in itself does not necessarily imply a cancellation of vertex corrections to optical conductivity.<sup>42</sup> Note also that the vertex corrections enhance conductivity (see also<sup>33</sup>) but suppress charge susceptibility.

To confirm that the origin of the difference between DMFT and FTLM in the optical conductivity is dominantly the vertex corrections term, we have evaluated the current-current correlation function  $\Lambda(iv_n)$  also in CTINT, and deduced the connected part by  $\Lambda^{\text{conn}}(iv_n) = \Lambda(iv_n) - \Lambda^{\text{disc}}(iv_n)$ , which is shown by the blue squares in Fig. 3c. These points fall precisely on the blue line which is obtained by analytical continuation of the difference in  $\sigma(\omega)$  between the FTLM and the DMFT  $4 \times 4$ . It is easy to check that  $\Lambda^{\text{conn}}(iv_n) \ll \Lambda^{\text{disc}}(iv_n) \approx \Lambda(iv_n)$ . However, by comparison of the correlation functions at the Matsubara frequencies only, one cannot easily judge on the importance of vertex corrections since the conductivity is determined by the slope,  $\sigma_{dc} = \sigma(\omega = 0) = -\partial_{iv} \text{Re} \Lambda(iv)|_{iv=0+}$ . The slope of the blue line is not small, and the bubble and the vertex corrections contributions to  $\sigma_{dc}$  are, in fact, comparable. We note that the structure of  $\Lambda^{\text{conn}}(iv)$  illustrates the difficulty of analytical continuation from the Matsubara to the real frequency axis, which we circumvented by using FTLM. The finite-size effect in the bubble term is the difference in  $\sigma(\omega)$  between DMFT and DMFT  $4 \times 4$  - its analytical continuation to the imaginary axis is presented with red lines and dots. We see that the corresponding slope at  $iv = 0$  is small, as expected. However, the magnitude at  $iv = 0$  is even bigger than that of the vertex corrections. Therefore,



to reconstruct the difference between FTLM and the (infinite lattice) DMFT on the imaginary axis (orange line), one needs to also take account of the finite-size effects in the bubble, even though it has little effect on  $\sigma_{dc}$ . Indeed, the sum of vertex corrections  $\Lambda^{\text{conn}}$  from CTINT and the difference between the DMFT and the DMFT  $4 \times 4$  (yellow diamonds) falls precisely on the orange line.

By now we have shown that at  $4 \times 4$ , the finite cluster size is irrelevant for the bubble, but can we make the same statement about the vertex corrections term? A priori, the contribution of vertex correction to  $\rho_{dc}$  may change with a growing cluster: the added longer distance components of  $\Lambda_r^{\text{conn}}$  might be sizeable, and even the short distance components might change due to improved diagrammatic content captured by the bigger cluster. As for the longer distance components, we analyze the vertex corrections term as a function of real-space vector  $\Lambda_r^{\text{conn}}(i\nu_n)$  and present the results in Fig. 3d. We observe that the value drops rapidly with distance and conclude that introducing further distance components will not affect the  $\mathbf{q} = 0$  value. As for the change in shorter distance components, we cannot make a definite statement, but we can observe what happens in the case of the self-energy. In Fig. 3a we see that the local self-energy does not change between the embedded single site and isolated  $4 \times 4$  cluster, and neither does the nearest-neighbor component of  $\Sigma$  between the embedded  $2 \times 1$  and isolated  $4 \times 4$  cluster. This gives us confidence that diagrams involving long-distance electron propagation are already negligible and that the vertex corrections term would not change with a further growth of the cluster. A similar conclusion was reached

in Ref.<sup>11</sup> where they studied cluster-size dependence of the  $\rho_{dc}$  result and found no change after size  $8 \times 8$  at temperatures relevant for our work, although they did not consider the  $4 \times 4$  size.

*Conclusions.* In summary, we carefully investigated the problem of high temperature transport for the Hubbard model on the square lattice. We have shown that long-range processes and non-local correlations make negligible contribution above a temperature  $T \sim 0.3D$  and hence the thermodynamic quantities and the one-particle spectral functions can be accurately calculated using the single-site DMFT approach. However, the vertex corrections to the conductivity persist to the highest examined temperatures and DMFT yields a reasonable, but quantitatively incorrect result for  $\sigma(\omega)$ . An essentially exact  $\sigma(\omega)$  can be computed using the exact diagonalization of an isolated  $4 \times 4$  cyclic cluster, which is in this regime quite representative of the thermodynamic limit.

## ACKNOWLEDGMENTS

We acknowledge useful discussions with Friedrich Krien. We acknowledge contributions and discussions with Ana Vranić and Jan Skolimowski at early stage of this project. JK,RŽ,JM are supported by Slovenian Research Agency (ARRS) under Program P1-0044 and Project J1-7259. JV and DT are supported by the Serbian Ministry of Education, Science and Technological Development under Project No. ON171017. Numerical calculations were partially performed on the PARADOX supercomputing facility at the Scientific Computing Laboratory of the Institute of Physics Belgrade. The CTINT algorithm has been implemented using the TRIQS toolbox<sup>43</sup>.

- <sup>1</sup> N. Barišić, M. K. Chan, Y. Li, G. Yu, X. Zhao, M. Dreschel, A. Smontara, and M. Greven, *Proceedings of the National Academy of Sciences* **110**, 12235 (2013).
- <sup>2</sup> S. Hartnoll, *Nature Phys.* **11**, 54 (2015).
- <sup>3</sup> S. A. Hartnoll, A. Lucas, and S. Sachdev, arXiv:1612.07324 (2016).
- <sup>4</sup> H. Terletska, J. Vučičević, D. Tanasković, and V. Dobrosavljević, *Phys. Rev. Lett.* **107**, 026401 (2011).
- <sup>5</sup> X. Deng, J. Mravlje, R. Žitko, M. Ferrero, G. Kotliar, and A. Georges, *Phys. Rev. Lett.* **110**, 086401 (2013).
- <sup>6</sup> W. Xu, K. Haule, and G. Kotliar, *Phys. Rev. Lett.* **111**, 036401 (2013).
- <sup>7</sup> J. Vučičević, D. Tanasković, M. J. Rozenberg, and V. Dobrosavljević, *Physical Review Letters* **114**, 246402 (2015).
- <sup>8</sup> N. Pakhira and R. H. McKenzie, *Phys. Rev. B* **91**, 075124 (2015).
- <sup>9</sup> E. Perepelitsky, A. Galatas, J. Mravlje, R. Žitko, E. Khatami, B. S. Shastry, and A. Georges, *Phys. Rev. B* **94**, 235115 (2016).
- <sup>10</sup> J. Kokalj, *Phys. Rev. B* **95**, 041110 (2017).

- <sup>11</sup> E. W. Huang, R. Sheppard, B. Moritz, and T. P. Devereaux, arXiv:1806.08346 (2018).
- <sup>12</sup> N. Hussey, K. Takenaka, and H. Takagi, *Philos. Mag.* **84**, 2847 (2004).
- <sup>13</sup> P. T. Brown, D. Mitra, E. Guardado-Sanchez, R. Nourafkan, A. Reymbaut, S. Bergeron, A. M. S. Tremblay, J. Kokalj, D. A. Huse, P. Schauss, and W. S. Bakr, arXiv:1802.09456 (2018).
- <sup>14</sup> N. Trivedi, R. T. Scalettar, and M. Randeria, *Phys. Rev. B* **54**, R3756 (1996).
- <sup>15</sup> G. Biroli and G. Kotliar, *Phys. Rev. B* **65**, 155112 (2002).
- <sup>16</sup> T. A. Maier, M. Jarrell, T. Pruschke, and M. H. Hettler, *Rev. Mod. Phys.* **77**, 1027 (2005).
- <sup>17</sup> G. Kotliar, S. Y. Savrasov, K. Haule, V. S. Oudovenko, O. Parcollet, and C. A. Marianetti, *Rev. Mod. Phys.* **78**, 865 (2006).
- <sup>18</sup> E. Gull, A. J. Millis, A. I. Lichtenstein, A. N. Rubtsov, M. Troyer, and P. Werner, *Rev. Mod. Phys.* **83**, 349 (2011).
- <sup>19</sup> J. P. F. LeBlanc, A. E. Antipov, F. Becca, I. W. Bulik,

- G. K.-L. Chan, C.-M. Chung, Y. Deng, M. Ferrero, T. M. Henderson, C. A. Jiménez-Hoyos, E. Kozik, X.-W. Liu, A. J. Millis, N. V. Prokof'ev, M. Qin, G. E. Scuseria, H. Shi, B. V. Svistunov, L. F. Tocchio, I. S. Tupitsyn, S. R. White, S. Zhang, B.-X. Zheng, Z. Zhu, and E. Gull, *Phys. Rev. X* **5**, 041041 (2015).
- <sup>20</sup> T. Ayrál and O. Parcollet, *Phys. Rev. B* **94**, 075159 (2016).
- <sup>21</sup> T. Ayrál, J. Vučičević, and O. Parcollet, *Phys. Rev. Lett.* **119**, 166401 (2017).
- <sup>22</sup> J. Vučičević, N. Wentzell, M. Ferrero, and O. Parcollet, *Phys. Rev. B* **97**, 125141 (2018).
- <sup>23</sup> G. Rohringer, H. Hafermann, A. Toschi, A. A. Katanin, A. E. Antipov, M. I. Katsnelson, A. I. Lichtenstein, A. N. Rubtsov, and K. Held, *Reviews of Modern Physics* **90**, 025003 (2018).
- <sup>24</sup> H. Hafermann, E. G. C. P. van Loon, M. I. Katsnelson, A. I. Lichtenstein, and O. Parcollet, *Phys. Rev. B* **90**, 235105 (2014).
- <sup>25</sup> R. Nourafkan, M. Cote, and A.-M. Tremblay, arXiv:1807.03855 (2018).
- <sup>26</sup> F. Krien, E. G. C. P. van Loon, M. I. Katsnelson, A. I. Lichtenstein, and M. Capone, arXiv:1811.00362 (2018).
- <sup>27</sup> A. Khurana, *Phys. Rev. Lett.* **64**, 1990 (1990).
- <sup>28</sup> N. Lin, E. Gull, and A. J. Millis, *Phys. Rev. B* **80**, 161105 (2009).
- <sup>29</sup> N. Lin, E. Gull, and A. J. Millis, *Phys. Rev. B* **82**, 045104 (2010).
- <sup>30</sup> D. Bergeron, V. Hankevych, B. Kyung, and A.-M. S. Tremblay, *Phys. Rev. B* **84**, 085128 (2011).
- <sup>31</sup> T. Sato, K. Hattori, and H. Tsunetsugu, *Phys. Rev. B* **86**, 235137 (2012).
- <sup>32</sup> N. Lin, E. Gull, and A. J. Millis, *Phys. Rev. Lett.* **109**, 106401 (2012).
- <sup>33</sup> T. Sato and H. Tsunetsugu, *Phys. Rev. B* **94**, 085110 (2016).
- <sup>34</sup> P. Coleman, *Introduction to Many-Body Physics* (Cambridge University Press, 2015).
- <sup>35</sup> J. Jaklič and P. Prelovšek, *Adv. Phys.* **49**, 1 (2000).
- <sup>36</sup> J. Jaklič and P. Prelovšek, *Phys. Rev. B* **52**, 6903 (1995).
- <sup>37</sup> A. N. Rubtsov and A. I. Lichtenstein, *J. Exp. Theor. Phys. Lett.* **80**, 61 (2004).
- <sup>38</sup> in FTL one can calculate self-energy, too, but it is beyond the generality of our implementation.
- <sup>39</sup> G. Kotliar, S. Y. Savrasov, G. Pálsson, and G. Biroli, *Phys. Rev. Lett.* **87**, 186401 (2001).
- <sup>40</sup> M. H. Hettler, A. N. Tahvildar-Zadeh, M. Jarrell, T. Pruschke, and H. R. Krishnamurthy, *Phys. Rev. B* **58**, R7475 (1998).
- <sup>41</sup> D. Poilblanc, *Phys. Rev. B* **44**, 9562 (1991).
- <sup>42</sup> The irreducible vertex in the ph-channel is  $\Gamma_{\text{ph}, \alpha\beta\gamma\delta} = \frac{\delta \Sigma_{\delta\gamma}[G]}{\delta G_{\alpha\beta}} \Big|_{G=G[G_0, \Sigma]}$  so even if a component of  $\Sigma$  is zero, it still depends on all components of the Green's function, and its derivative is not necessarily zero.
- <sup>43</sup> O. Parcollet, M. Ferrero, T. Ayrál, H. Hafermann, P. Seth, and I. S. Krivenko, *Comput. Phys. Commun.* **196**, 398 (2015).